Bovine serum albumin protected Cd8 nanoclusters as efficient two-photon absorbers for near-infrared excited fluorescence imaging of intracellular pH

Yuchi Cheng, Yu Zhao, Hao Yuan, Huangmei Zhou, Jinming Xu, Xihang Chen, Kun Zhang, Rodolphe Antoine, Sanjun Zhang

TWO MAJOR COMMENTS:

-MALDI-MS spectra are not convincing and should be removed or more convinving spectra should be reported.

-Long lifetime microscend components should be better addressed.

Bovine Serum Albumin Protected Cadmium Nanoclusters as Efficient Two-photon Absorbers for Near-infrared Two-photon Excited Fluorescence Imaging of Intracellular pH

Yuchi Cheng [a], *Yu Zhao* [a], *Huangmei Zhou* [a], *Jinming Xu* [a], *Xihang Chen* [a], *Hao Yuan* [b], *Kun Zhang*[c], *Rodolphe Antoine* [b,] **, and Sanjun Zhang* [a, d,] ***

[a] State Key Laboratory of Precision Spectroscopy, East China Normal University, No.500, Dongchuan Road, Shanghai 200241, China

[b] Institut Lumière Matière UMR 5306, Université Claude Bernard Lyon 1, CNRS, Univ Lyon, F69100 Villeurbanne, France

[c] Shanghai Key Laboratory of Green Chemistry and Chemical Processes, College of Chemistry and Molecular Engineering, East China Normal University, No.3663, North Zhongshan Road, Shanghai 200062, China

[d] Collaborative Innovation Center of Extreme Optics, Shanxi University, Taiyuan, Shanxi 030006, China

*Correspondence to R.A (email: rodolphe.antoine@univ-lyon1.fr) and S.Z. (email: sjzhang@phy.ecnu.edu.cn)

Abstract

Metal nanoclusters-based fluorescent sensors have made great progress in the field of analytical chemistry, but their practical applications in biological sensing were limited by poor (photo)stability and restricted excitation wavelengths in the UV-visible range and low quantum yields. It is of great significance to develop near-infrared excited metal nanoclusters-based fluorescent sensors with high quantum yield. In contrast to noble metal nanoclusters (e.g., Au, Ag, and Pt), stable and affordable fluorescent metal nanoclusters have received relatively less attention in research, except for Cu nanoclusters. Herein, we developed a rapid one-pot route to synthesize high cadmium content nanoclusters (CdNCs) employing bovine serum albumin (BSA) as both reducing and templating agents. The obtained CdNCs displayed bright fluorescence emission with quantum yield of 13.8%. Of particular interest, the CdNCs demonstrated remarkable proficiency as two-photon absorbers, displaying a two-photon absorption (TPA) cross section of up to 1076 GM (excited at 730 nm), higher than TPA cross section of BSA-protected AuNCs and also surpassing that of conventional dyes by two orders of magnitude. Additionally, the CdNCs exhibited pH-sensitive photoluminescence, and the pH-responsive mechanism was revealed by time resolved fluorescence spectroscopy, transient absorption spectroscopy, etc. Benefiting from protein coating, CdNCs exhibited excellent biocompatibility and were successfully utilized as two-photon excited fluorescence sensors for intracellular pH.

Keywords: Cadmium nanoclusters, Nonlinear optics, Excited state dynamics, Two-photon excited imaging, pH sensor

1. Introduction

Fluorescent sensors are powerful tools for the monitoring of various biological parameters, such as pH, ionic concentrations, and metabolites (Han and Burgess, 2010; Wu, D. et al., 2017; Zhao et al., 2015). As a sensitive, and noninvasive bioanalytical method with a high time-spatial resolution, the fluorescence sensor-based imaging

technique allows the visual tracking and quantification of intracellular substances, which has revolutionized the way of understanding biological events in living systems (Ashton et al., 2015).

To date, many fluorescent sensors based on different materials (such as organic molecules, fluorescent proteins, quantum dots, and metal nanoclusters) have been established for cell imaging (Algar et al., 2021). From a practical point of view, the ideal fluorescent biosensor should have a small size, bright and stable luminescence, good biocompatibility, easy synthesis, and low cost. In recent years, ligand-protected metal nanoclusters (MNCs) have attracted great attention due to their simple synthesis, adjustable luminescence, and good photostability (Qiao et al., 2021). Moreover, metal nanoclusters could inherit the good properties of the ligands, such as water solubility, biocompatibility and functional groups, making them potential nanomaterials for the construction of fluorescent sensors (Qian et al., 2022; Sobhan Chatterjeea, 2022). Compared with small molecules or polymers as ligands, proteins have gained considerable attention for their better structural stability, metal affinity, biocompatibility and functionality (Guo et al., 2021; Xavier et al., 2012)[Bonačić-Koutecký, V.; Le Guével, X.; Antoine, R., Engineering Liganded Gold Nanoclusters as Efficient Theranostic Agents for Cancer Applications. *ChemBioChem* **2023**, *24*, e202200524; Antoine, R.; Maysinger, D.; Sancey, L.; Bonačić-Koutecký, V., Open Questions on Proteins Interacting with Nanoclusters. *Communications Chemistry* **2022**, *5*, 47.].

Since Xie et al. successfully demonstrated biomineralized synthesis of photoluminescent BSA-protected gold nanoclusters (BSA-AuNCs) (Xie et al., 2009), multifarious proteins had been used to synthesize metal nanoclusters, which were further employed as fluorescent sensors (Ghosh et al., 2014; Hu et al., 2012; Niu et al., 2021; Shi et al., 2015; Wang et al., 2018; Wang and Xiao, 2021). Nevertheless, most protein-directed synthesized MNCs have low quantum yields and UV-visible excitation wavelengths, limiting the practical application in biological imaging (Iman Zare, 2021), even if recent strategies aiming at tailoring the NIR-II

photoluminescence of gold nanoclusters has been proposed by selective binding to protein [F. Bertorelle, K. D. Wegner, M. Perić Bakulić, H. Fakhouri, C. Comby-Zerbino, A. Sagar, P. Bernadó, U. Resch-Genger, V. Bonačić-Koutecký, X. Le Guével, R. Antoine, *Chem. Eur. J.* **2022**, *28*, e202200570.].. Meanwhile, most protein-protected MNCs were composed of noble metals, such as Au, Ag, and Pt, whose precursor materials are relatively expensive. And there have been far fewer MNCs prepared using low-cost metal (Fe, Ni, and Cd) as precursors, due to the relatively complicated synthesis, and their unsatisfactory optical properties and stability (Goswami et al., 2014; Harshita et al., 2023; Ivleva et al., 2020; Sarparast et al., 2016; Wang et al., 2023). Although Cu nanoclusters have also been reported, the stability of water-soluble CuNCs still needs to be further improved (Hu et al., 2017; Li et al., 2017; Miao et al., 2016). Therefore, it is of great significance to develop low-cost, stable protein-protected metal nanoclusters with high quantum yield and near-infrared (NIR) excitation wavelengths.

Many efforts have been made to overcome these challenges. Metal doping is a promising strategy for increasing quantum yield (Mohanty et al., 2012), and Tang et al. enhanced the fluorescence intensity of BSA-AuNCs by controlling the proportion of doped Ag ions (Zhou et al., 2016). The introduction of additional ligands can also enhance the fluorescence of clusters (Niu et al., 2021), Chang et al. successfully synthesized brighter BSA/GSH-AuNCs using GSH as auxiliary ligands (Wu, B.Y. et al., 2017). The increase of the ligand structure rigidity has been proven to significantly enhanced the fluorescence quantum yield of MNCs (Maity and Kumar, 2022; Wei et al., 2019). Moreover, there were limited reports on the bright NIR-excited MNCs. Recently, MNCs have been demonstrated to be efficient two-photon absorbers in numerous literatures (Bonacic-Koutecky and Antoine, 2019; Olesiak-Banska et al., 2019; Ramakrishna et al., 2008; Russier-Antoine et al., 2014), suggesting that the excitation wavelengths could be conveniently extended to the NIR region by two-photo excited fluorescence. The two-photon absorption (TPA) cross-section value for BSA with one Au8NCs was obtained to be 190 GM and 540

GM for BSA with three Au8NCs, at 740 nm excitation wavelength. [Kindi, H. A.; Mohamed, A.; Kajimoto, S.; Zhanpeisov, N.; Horino, H.; Shibata, Y.; Rzeznicka, I. I.; Fukumura, H., Single Bovine Serum Albumin Molecule Can Hold Plural Blue-Emissive Gold Nanoclusters: A Quantitative Study with Two-Photon Excitation. *Journal of Photochemistry and Photobiology A: Chemistry* **2018**, *357*, 168-174.] Consequently BSA-protected AuNCs were reported to be good candidates for multi-photon imaging. [1. Raut, S. L.; Shumilov, D.; Chib, R.; Rich, R.; Gryczynski, Z.; Gryczynski, I., Two Photon Induced Luminescence of Bsa Protected Gold Clusters. *Chemical Physics Letters* **2013**, *561-562*, 74-76.]

In this work, we synthesized a novel water-soluble CdNCs through a rapid and simple route, using BSA acting as both reducing and templating agents and $CdCl_2$ as the metal precursors. The morphology, size, basic and nonlinear optical properties of CdNCs were characterized. The synthesized CdNCs showed pH-sensitive fluorescence emission, and the relevant excited state dynamics was elucidated. Finally, the CdNCs have been successfully applied in intracellular pH sensing under NIR excitation due to their excellent two-photon fluorescence property and biocompatibility. To our knowledge, this was the first time to report the nonlinear optical properties and excited state dynamics of protein directed-CdNCs. This work held the potential to offer a new perspective on the design and development of stable, low-cost nanocluster-based sensors under near-infrared excitation.

2. Material and methods

2.1. Materials and reagents

Cadmium chloride ($CdCl_2$, 99%) was purchased from Fisher Chemical (USA), Bovine serum albumin, Dulbecco's Modified Eagle Medium (DMEM) and nigericin were purchased from Sigma-Aldrich Chemical Reagent Co., Ltd. (Shanghai, China). Metal ions, amino acids, NaCl, KCl, Na_2HPO_4, NaH_2PO_4 and K_2HPO_4 were obtained from Sinopharm Chemical Reagent Co., Ltd. (Shanghai, China). Glucose and methyl thiazolyl tetrazolium (MTT) were obtained from Tokyo Chemical Industry Co., Ltd. HEPES was purchased from Amresco (Shanghai, China). The dialysis tube (MWCO:

1000 Da) was obtained from VAKE Corporation (Beijing, China). All chemicals from commercial sources were used without further purification. All aqueous solutions were prepared with ultrapure water (18.2 MΩ · cm).

2.2. Instrumentation

The absorption spectra were measured with UV–Vis spectrometer (TU-1901, PERSEE, China). The steady-state fluorescence spectra were obtained by a fluorescence spectrometer (FluoroMax-Plus, Horiba, Japan). Fluorescence lifetimes were measured with a homemade time-correlated single photon counting system, a 405 nm semiconductor laser with adjustable repetition frequency and the picoHarp 300 (PicoQuant, Germany) were used as excitation light and single photon counting module respectively. Two-photon absorption cross section were measured by a self-built Z-Scan system with a 1 KHz femtosecond laser (COHERENT, USA). Transient absorption spectra were measured by a commercial transient absorption spectrometer (Helios Fire, USA). Transmission electron microscopic (TEM) images were collected on a transmission electron microscope (JEM-2100F, JEOL, Japan). Fourier transform infrared (FTIR) spectra were performed with an infrared spectrometer (NICOLET iS10, Thermo Fisher Scientific, USA). UV circular dichroism (CD) spectra were obtained using a spectropolarimeter (J-1500, Jasco, Japan). Mass spectra were recorded in a matrix-assisted laser desorption ionization time-of-flight mass spectrometer (MALDI-TOF MS) (Autoflex-TOF, Bruker Daltonics, USA). All experiments were carried out at room temperature unless otherwise noted.

2.3. Synthesis of CdNCs and AuNCs

The CdNCs were synthesized according to previously reported with a little modification (Sarparast et al., 2016). Briefly, $CdCl_2$ aqueous solution (20 mM, 2 mL) was added into 2 mL BSA solution (25 mg/mL). After stirring for 2 min, NaOH (1 M) solution was added to adjust the pH to 12, keep stirring for another 3 min. Finally, the mixture was stirred at 70℃ for 1 h. The synthesized nanoclusters were dialyzed in PBS (pH 7.4) for 24 h, and the dialysate was changed every 8 h (MWCO: 1000 Da).

The CdNCs were stored at 4℃.

The BSA-AuNCs were synthesized according to previously reported (Xie et al., 2009), then further purified by dialysis (MWCO: 1000 Da) and stored at 4℃.

3. Results and discussion

3.1. Synthesis and characterization of CdNCs

BSA is a common commercial protein, rich in groups with affinity for metals, such as -COOH, -NH_2 and -SH, which are conducive to the formation of stable metal complex structure. As many literatures reported that, fluorescent BSA protected MNCs can be synthesized based on the reducing property of tyrosine (Tyr) under alkaline conditions, without strong reductant (Xavier et al., 2012; Xie et al., 2009). The synthesis efficiencies of MNCs are significantly affected by the standard reduction potentials of metal ions. Compared with Au and Ag (1.83 V and 0.799 V), the standard reduction potential of Cd is lower (-0.402 V), meaning that the biomineralized synthesis of fluorescent BSA-protected CdNCs was challenging. Although, Mir F. Mousavi et al. successfully synthesized fluorescent BSA-CdNCs with excitation and emission wavelengths of 360 nm and 475 nm, with quantum yield of 2.86% (Sarparast et al., 2016). However, the ultraviolet excitation wavelength, low quantum yield and long reaction time limited its wide application in bioimaging. Therefore, the rapid synthesis of BSA-CdNCs with redder excitation wavelength and higher quantum yield is of great significance.

Herein, we synthesized bright fluorescent CdNCs with BSA as ligands and $CdCl_2$ as metal precursor. Firstly, the effects of reactant ratio, initial pH, and incubation time on the fluorescence properties of the synthesized CdNCs were investigated. As BSA concentration, reaction pH and incubation time were fixed, the input $CdCl_2$ concentration significantly affected the fluorescence intensity of obtained products. While Cd^{2+} increased from 5 mM to 20 mM, the fluorescence intensity of products gradually increased due to the incorporation of more cadmium within BSA , and the spectral shape was basically unchanged (Figure S1a). When the concentration of Cd^{2+} increased to 25 mM, the fluorescence intensity decreased slightly with a redshift of

emission spectrum showing the limiting concentration for cluster synthesis. Subsequently, we investigated the influences of reaction pH and incubation time. No obvious fluorescent products generated when reaction pH was lower than 10, because the reducing capability of Tyr (pKa ~10) was greatly inhibited (Xie et al., 2007). Upon adjusted pH to be more basic, products with fluorescence emission could be rapidly obtained (Figure S1b). By controlling multiple parameters in the synthesis process, we successfully synthesized CdNCs with intense fluorescence emission (Scheme 1). Simply, after adding Cd^{2+} into the BSA aqueous solution, the protein molecules would capture Cd^{2+} and activated the reducing capability of Tyr by adjusting the reaction pH to 12. The encapsulated Cd^{2+} were gradually reduced to form CdNCs, and the whole reaction took only 1 hour, which showed a higher efficiency compared with previous reports (Ivleva et al., 2020; Sarparast et al., 2016).

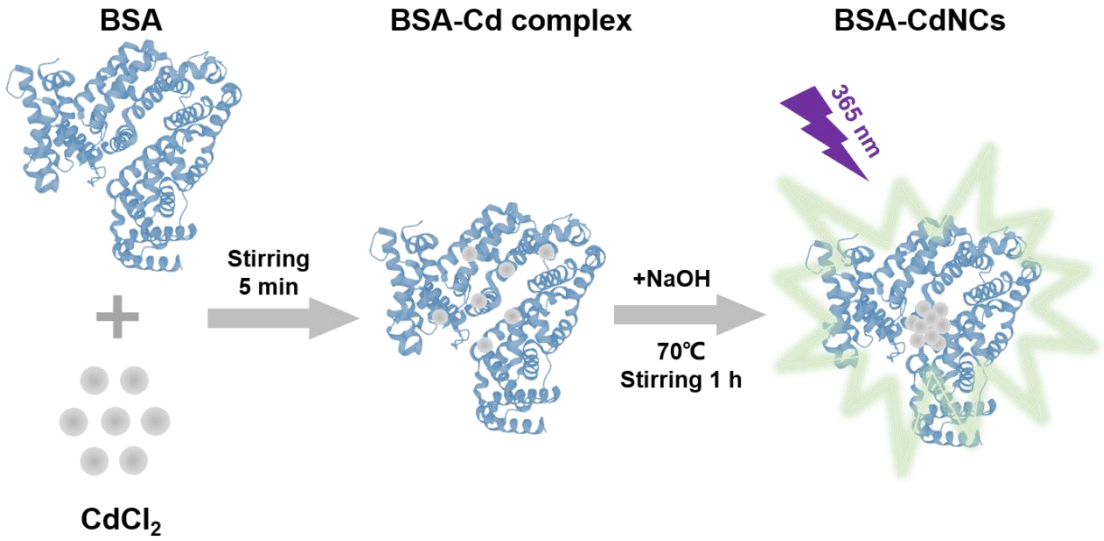

Scheme 1. Schematic illustration of the synthesis of photoluminescent CdNCs.

To confirm the formation of CdNCs, the fluorescence spectra of BSA and BSA-Cd^{2+} complex were measured, BSA and BSA-Cd^{2+} complex showed no obvious fluorescence emission under 365 nm excitation (Figure S2a). It indicated that the obtained fluorescent products were not BSA-Cd^{2+} complexes, but due to the formation of CdNCs. As shown in Figure. 1a, the synthesized CdNCs exhibited an obvious fluorescence emission at around 515 nm under 365 nm excitation, and there were two characteristic absorption bands between 250 nm and 400 nm. The

absorption peak of native BSA located at 278 nm, and the BSA-Cd complex has a wide absorption band in the range of 300-350 nm, suggesting the characteristic absorption at 360-400 nm was related to the formation of the CdNCs (Figure S2b). Indeed, looking at the cadmium sulfide series obtained in the literature, upon going to the larger clusters, the first band progressively redshifts to 326 nm and 351 nm (in DMF) for [Cd32S14(SPh)40]4− and [Cd54S32(SPh)48(H2O)4]4−, respectively.[http://dx.doi.org/10.1063/1.4922320] BSA protein possesses 34 sulfide atoms (involved in disulfide bonds) and one free sulfide atom in cys34 residue, thus Cd clusters (protected by sulfides) with sizes higher than 50 atoms may be produced displaying similar near-UV absorption. The influence of the CdNCs formation on the BSA structure was scrutinized by FTIR spectroscopy (Figure 1b). After CdNCs formation, the absorption peaks corresponding to S-H, C-H, N-H and O-H in the range of 2500-4000 cm^{-1} were significantly weakened, indicating that the nanoclusters structure was stabilized by the combination of -SH, -COOH and -NH_2 with Cd atoms. The reduction of the amide bands-related characteristic absorption of native BSA (1050-2000 cm^{-1}), suggested the conformational changes in the protein (Sarparast et al., 2016). The FTIR spectral shape of CdNCs was consistent with that of native BSA, indicating that the nanoclusters retain most basic properties of the protein, which was conducive to further functionalization and biomedical applications. The morphology and size of CdNCs were characterized by TEM. The synthesized CdNCs showed obvious cluster structure with an average diameter of ~3.2 nm (Figure 1c). MALDI-TOF MS showed the CdNCs molecular weight to be ~74 kDa (Figure 1d), which was increased by ~7.5 kDa from native BSA (~66.36 kDa) [Chem. Eur. J. 2022, 28, e202200570.]. CdNCsCdNCsCompared with previously reported Cd_{41}NCs with fluorescence emission peak at 500 nm (Ivleva et al., 2020), the as-synthesized CdNCs are expected to have a larger metal core and the emission peak redshifted to ~515 nm, which was consistent with quantum size effect (Zheng et al., 2004). The fluorescence quantum yield of CdNCs was ~13.8% at pH 6.0 (Ex@365 nm) using quinine sulfate (54%) as reference (Figure S3). Compared with other

protein-protected metal nanoclusters (Iman Zare, 2021), CdNCs showed a higher quantum yield, which was 5-fold higher than the previous report (Sarparast et al., 2016), suggesting that it was more suitable for bioimaging.

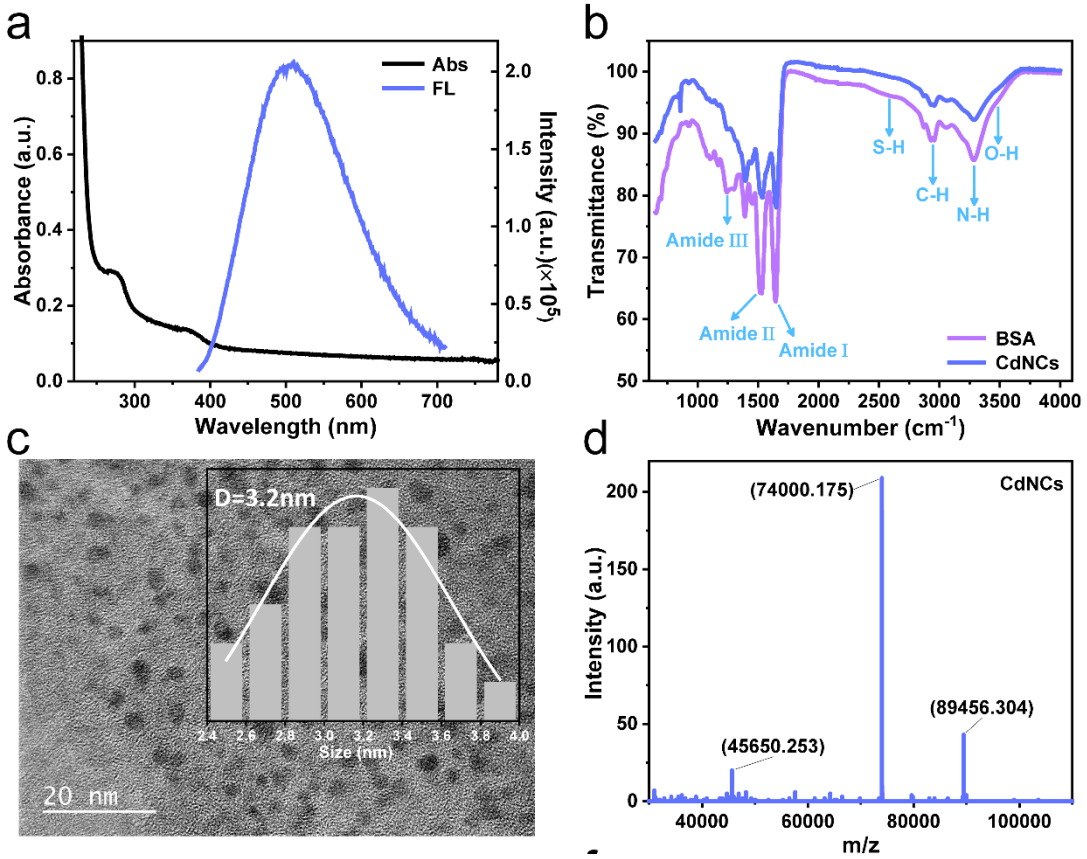

Figure 1. Characterization of CdNCs. (a) Absorption and fluorescence emission spectra of CdNCs excited at 365 nm. (b) FT-IR spectra of native BSA and CdNCs. (c) TEM image of CdNCs, illustration: the size statistics of CdNCs. (d) MALDI-TOF mass spectrum of CdNCs.

3.2. Mechanism of pH regulating fluorescence emission of CdNCs

It was found rthat CdNCs also exhibited pH-dependent photoluminescence. Fluorescence spectra of CdNCs at different pH values were measured (Figure 2a), when the pH increased from 6.0 to 10.5, the fluorescence intensity of CdNCs decreased by about 3 times. Simultaneously, the time-resolved fluorescence decay spectra of CdNCs were also pH-responsive (Figure 2b). As the pH raised, the proportion of fast components in the fluorescence decay process of CdNCs increased,

and the fluorescence average lifetime decreased from ~130 ns to ~90 ns (Table S1). Such results implied that CdNCs have the potential to be fluorescence intensity or fluorescence lifetime pH sensors.

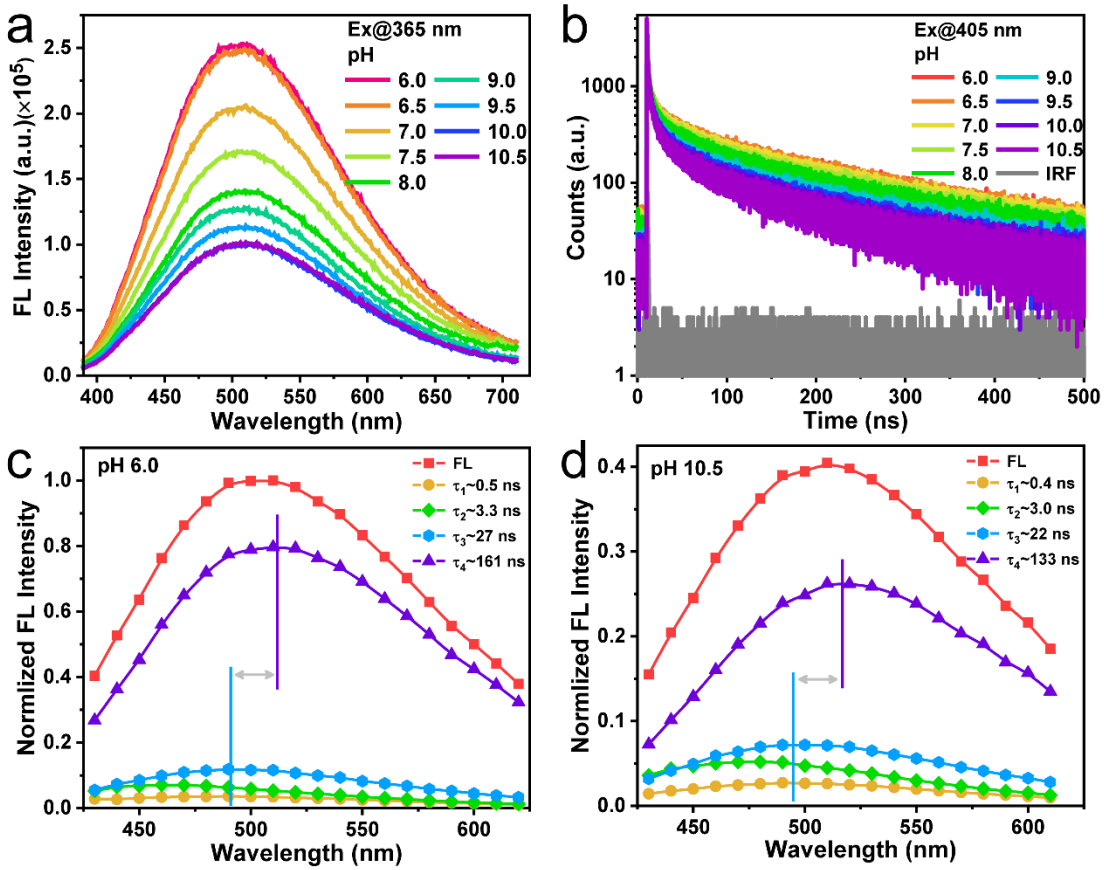

Figure 2. pH-sensitive fluorescence emission of CdNCs. (a) Emission spectra of CdNCs at different pH values excited at 365 nm. (b) Time-resolved fluorescence decay spectra of CdNCs at different pH values under 405 nm excitation. (c, d) Decay associated fluorescence spectra of CdNCs at pH 6.0 and 10.5, the intensities were normalized to the peak intensity at pH 6.0.

We furtherly explored the regulation mechanism of pH. From the absorption spectra of CdNCs at different pH values (Figure S4a), the increase of pH caused a slight decrease in the absorption around 280 nm, while the absorption band remained unchanged at 300-400 nm, indicating that the metal core structure of CdNCs kept steady. The pH-dependent excited state dynamics of CdNCs were investigated to elucidate the photophysical process. The time-resolved fluorescence decay spectra of CdNCs at a series of emission wavelengths were measured, then globally fitted with a multi-exponential decay model. Four lifetime components were obtained: τ_1~0.5 ns,

τ_2~3 ns, τ_3~25 ns, τ_4~150 ns. Combined with steady-state fluorescence spectra, the decay associated fluorescence spectra (DAS) of CdNCs at pH 6.0 and 10.5 were constructed. As shown in Figure 2c and 2d, the overall contribution of each lifetime was different, and the longer lifetime contributed more to the total fluorescence. Compared with the τ_3 component, τ_4 was the main source of fluorescence emission. Two short lifetime components (τ_1, τ_2) hardly contributed to fluorescence intensity, which may represent some non-radiative transition processes. Notably, the fluorescence emission of τ_4 exhibited ~25 nm redshift with respect to τ_3, meaning the existence of two different emission states. When pH increased from 6.0 to 10.5, the intensity of the τ_4 decreased by a factor of ~3, which agreed well with the amplitude of steady-state fluorescence intensity, indicating that this component was the main origin of the pH responsive fluorescence of CdNCs. Tang et al. observed a fast nanosecond component and a slow microsecond component in the fluorescence dynamics of BSA-AuNCs, and attributed them to the prompt fluorescence (PF) from excited singlet states and the delayed fluorescence (DF) involving reversible intersystem crossings (ISC) between singlet and triplet states (Wen et al., 2012). By measuring fluorescence dynamics at different emission wavelengths, Tang et al. proposed that there was a large spectral overlap between PF and DF, and DF has a redder emission. Meanwhile, DF has a longer lifetime than PF due to the thermal equilibrium between singlet and triplet states. Furthermore, the method for calculating the triplet formation yields (η_{S-T}) of BSA-AuNCs was provided (Wen et al., 2012). On this basis, we proposed τ_2, τ_3 and τ_4 components in CdNCs may correspond to the ISC, PF and DF processes. The η_{S-T} of CdNCs at different pH values were further calculated (Figure S4b), which gradually decreased with increasing pH, weakening the DF emission. It has been reported that the formation of excited triplet states was related to the complex of Au(I) and ligands in the Au(I)-S semicyclic motifs on the AuNCs surface (Wang et al., 2004) and also protected by BSA tempaltes [*Chem. Eur. J.* **2022**, *28*, e202200570]. For CdNCs, Cd-S motifs were mainly formed by interacting between Cd ions and cysteine (Cys) residues in BSA (Sarparast et al.,

2016). Cysteines were added to CdNCs to form more Cd-S motifs. Interestingly, the addition of Cys induced the absorption spectrum of CdNCs an opposite change to that when increasing pH (Figure S5a), the absorption around 280 nm was slightly enhanced and the absorption band at 300-400 nm was still unchanged. Meanwhile, the introduction of Cys increased the emission intensity and fluorescence lifetime of CdNCs (Figure S5b and S5c). The DAS showed that the addition of Cys mainly led to the increase of DF emission, indicating that the excited triplet state of CdNCs was indeed related to the surface Cd-S motifs (Figure S5d). We measured the η_{S-T} of CdNCs at different emission wavelengths after adding Cys and increasing pH (Figure S6a). The introduction of Cys led to the increase of η_{S-T}, which was contrary to the result caused by an increase in pH. As previously reported that pH could change the structure of BSA (Cao et al., 2013). CD spectra were used to expound the structural changes of CdNCs at different pH values (Figure S6b). The native BSA has two negative bands at 210 nm and 222 nm, which were characteristics of the α-helix structure of proteins (Greenfield, 2006). After CdNCs formation, the absorption at these wavelengths decreased significantly, and a positive band appeared around 210 nm, indicating the decrease of α-helix content and the increase of random coil structures (Cao et al., 2013). As the pH increases, the BSA exhibited looser structures, which may affect the Cd-S motifs of nanoclusters, leading to the reduction of the quantum yields of triplet formation, and ultimately reducing the fluorescence intensity and lifetime.

The femtosecond and microsecond transient absorption spectra were measured at different pH to fully reveal the photocycle of CdNCs. As shown in Figure 3, the transient absorption spectra of CdNCs had obvious negative signal below 400 nm, whose positions agreed well with the steady-state absorption spectrum of CdNCs, representing ground-state bleaching (GSB). A broad positive signal located in the range of 400-650 nm, corresponding to excited state absorption (ESA) of CdNCs. No significant stimulated emission (SE) band was observed, probably overlapped with broad ESA. At pH 6.0 and 10.5, CdNCs experienced similar relaxation process within

the initial 7 ns after excited at 365 nm (Figure 3a and S7a). During the first 2 ps, the kinetic curves at 510 nm and 635 nm decayed rapidly, and the signal at 402 nm raised simultaneously (Figure 3d and S7b). From the time-evolution of the femtosecond transient absorption spectra (Figure S8a), ESA around 402 nm unabated but slightly blue shifted with the decrease of ESA in the range of 430 to 650 nm. There was no obvious isosbestic point probably due to the large overlap between two ESA bands. At the same time, GSB showed a slight weakening during this process due to the overlap with the ESA around 402 nm. In the next 7 ns, both ESA and GSB decayed, and the transient spectral feature changed obviously. ESA band around 402 nm exhibited a faster decay rate (Figure S8b and S9a). Three time-constants were obtained from the decay dynamics of 402 nm, 510 nm and 635 nm: ~ 1 ps, ~ 100 ps and ~ 2.5 ns (Figure S9a). The time-constant ~1 ps corresponding to the initial rise at 402 nm and the decay of 510 nm, 635 nm, could be assigned to the internal conversion (IC) between higher and lower excited state levels (Zhou and Jin, 2021), whereas the 100-ps decay may represent the nonradiative relaxation associating with the τ_1 component of DAS spectra. Meanwhile, the 2.5-ns lifetime consistent with the τ_2 obtained from the time-resolved fluorescence decay spectra, was assigned to the ISC process (Wen et al., 2012). Moreover, the decay curve at 402 nm had an extra lifetime of ~5.5 ps, which may involve the charge transfer (CT) among the metal core and the surface ligand motifs (Qian et al., 2010) or solvation (Zhou and Jin, 2021). The dynamic processes of CdNCs on the microsecond scale were relatively simple (Figure 3b and 3c), both ESA and GSB decayed slowly (Figure 3e and 3f), and the transient spectra features remained almost unchanged (Figure S7c and S7d). Four lifetime components were obtained through global analysis, In addition to three components consistent with the DAS results, there was an extra microsecond lifetime component (Figure S9b, Table S2). When pH increased from 6.0 to 10.5, the microsecond lifetime decreased from 1500 ns to 830 ns, and the proportion in the GSB decay process increased (Table S2). This component was present in GSB but not observed in time-resolved fluorescence decay spectra, which may be related to the non-radiative transition from excited triplet

state to ground state.

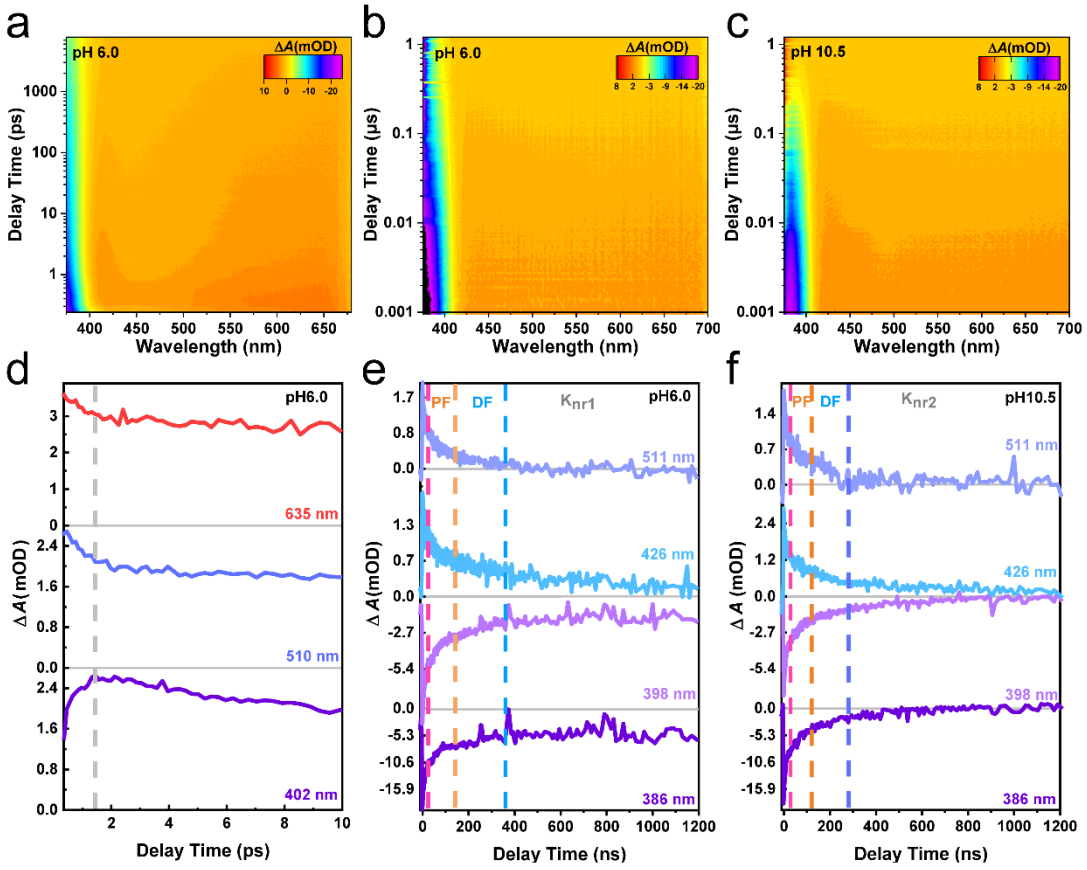

Figure 3. Transient absorption spectra of CdNCs. (a) Femtosecond transient absorption spectra of CdNCs at pH 6.0. (b, c) Microsecond transient absorption spectra of CdNCs at different pH. (d-f) Excited state kinetic curves of CdNCs at different time scales at pH6.0 and 10.5.

Thus, we proposed the possible photocycle of CdNCs at different pH (Scheme 2). CdNCs arrived at a high-level excited state (S_n) after 365 nm pumping, and cooled down to a low-level excited state (S_1) through internal conversion (IC) within 2 ps. One part of S_1 population would transit to triplet states by intersystem crossings (ISC). Another part relaxed to the ground state (S_0) in the form of PF (~20 ns) at ~495 nm. The excited triplet state either reverse intersystem crossed (RISC) to S_1 and emitted DF (~150 ns) at ~515 nm or returned to the S_0 through long-term non-radiative relaxation (~1000 ns). The increase of pH value induced the conformational changes of BSA, which affected Cd-S motifs in CdNCs, reduced the quantum yields of triplet formation and enhanced the non-radiative transition channels, finally weakened the fluorescence of CdNCs. The quantum yield of CdNCs decreased to ~3.8% at pH 10.5

(Figure S3), suggesting that the enhancement of non-radiative transition channel under alkaline condition.

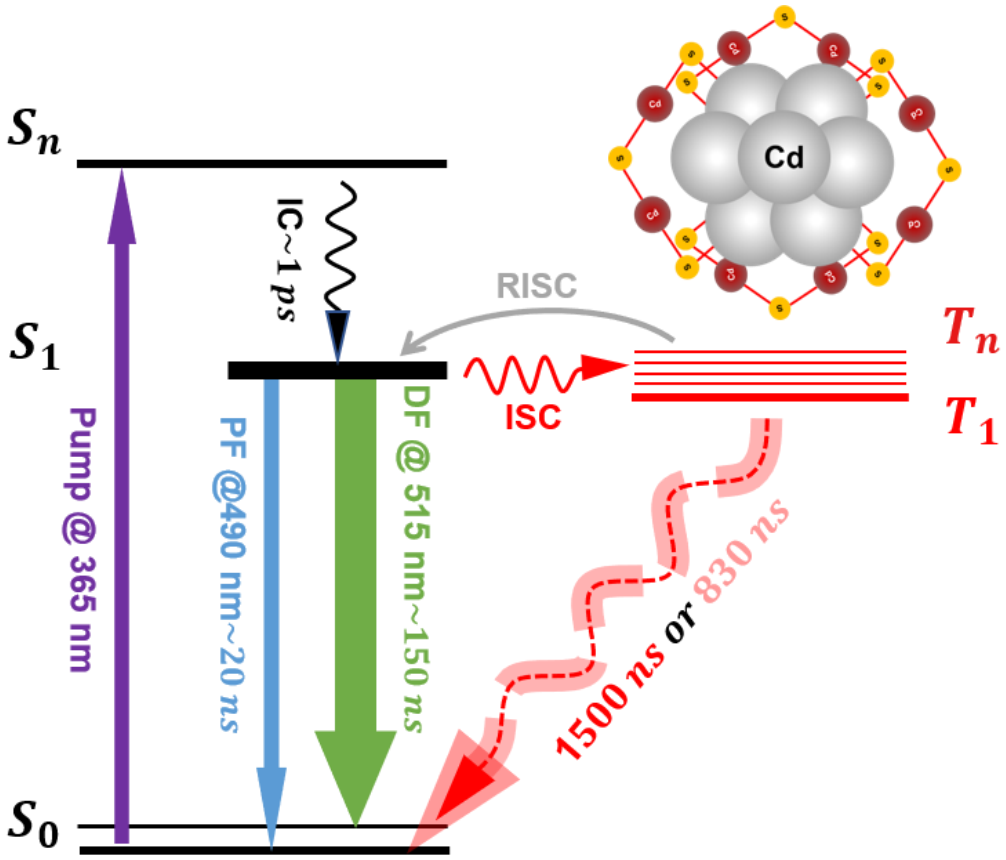

Scheme 2. Simplified photocycle model of CdNCs.

3.3. Two-photon absorption and two-photon excited fluorescence

In recent years, many researches have reported the excellent nonlinear optical properties of MNCs (Olesiak-Banska et al., 2019; Wei et al., 2022)[DOI https://doi.org/10.1039/C4NR03782K] [Bonačić-Koutecký V, Antoine R. Enhanced two-photon absorption of ligated silver and gold nanoclusters: theoretical and experimental assessments. Nanoscale 11, 12436-12448 (2019)], promising to extend the excitation wavelengths to the NIR window by multiphoton excitation fluorescence, avoiding the UV irradiation induced endogenous fluorescence and cell phototoxicity during bioimaging. [Bonačić-Koutecký, V.; Le Guével, X.; Antoine, R., Engineering Liganded Gold Nanoclusters as Efficient Theranostic Agents for Cancer

Applications. *ChemBioChem* **2023**, *24*, e202200524; Antoine, R.; Maysinger, D.; Sancey, L.; Bonačić-Koutecký, V., Open Questions on Proteins Interacting with Nanoclusters. *Communications Chemistry* **2022**, *5*, 47.]. Two-photon absorption cross section is an important parameter to describe the nonlinear optical properties of fluorescent biosensors. Two-photon excitation (TPE) fluorescence is a highly sensitive method to determine the two-photon absorption (TPA) cross sections of fluorescent materials (Xu and Webb, 1996). As shown in Figure. 4a, the CdNCs had obvious fluorescence emission under excitation at 800 nm, and the emission spectra were basically consistent with that under single photon excitation. The emission intensity of CdNCs showed excitation power dependence with corresponding slopes close to 2 indicating that the emission was two-photon induced fluorescence (Figure 4b) (Xu and Webb, 1996). Using fluorescein as reference (Albota et al., 1998), the TPA cross section of CdNCs at 800 nm and 730 nm was calculated to be 468 GM and 1076 GM respectively, which were two orders of magnitude higher than that of common dyes (Makarov et al., 2008), meaning that the synthesized CdNCs were efficient two-photon absorbers. Taking the advantages of high quantum yield and large TPA cross section, CdNCs were potential candidates for two-photon fluorescence imaging.

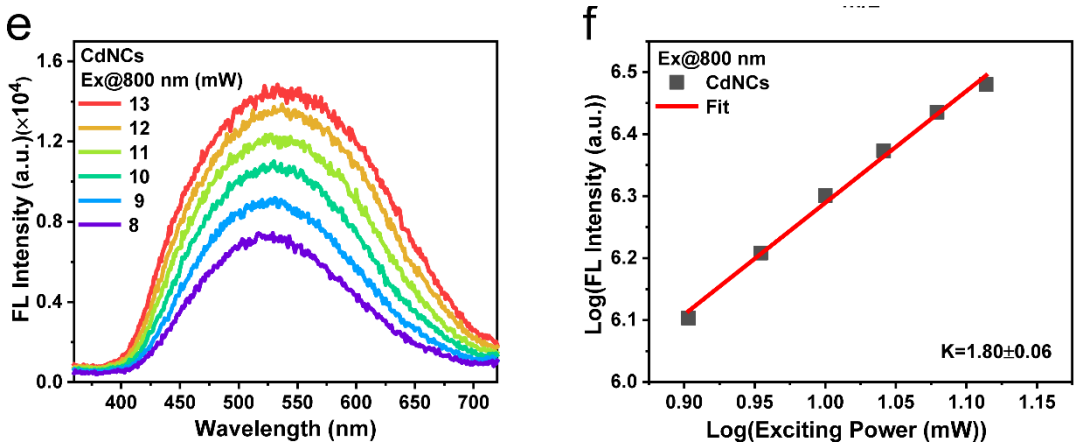

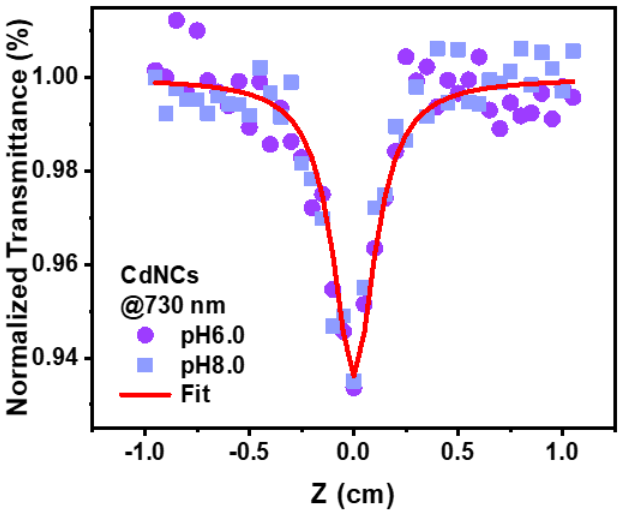

Figure 4: (e) Two photon emission spectra of CdNCs at different excitation powers (Ex@800 nm). (f) Relationships between the fluorescence intensity and the excitation power of CdNCs under 800 nm excitation. (g) Measurement of two-photon absorption cross sections of CdNCs at 730 nm under different pH values obtained from the home-built Z-Scan system.

3.4. Two-photon excited fluorescence imaging of intracellular pH

Based on the high fluorescence quantum yield, large TPA cross sections and pH-sensitive fluorescence, CdNCs were expected to be two-photon excited fluorescence sensors for intracellular pH. Firstly, the cytotoxicity of CdNCs was evaluated when incubated into living cells, due to the inherent biological toxicity of Cd metal atoms. Many literatures have reported that BSA-protected metal nanoclusters could be applied in biomedicine and bioimaging as low-cytotoxicity nanomaterials because of the encapsulation of metal atoms by BSA (Dong et al., 2015; Iman Zare, 2021; Ivleva et al., 2020). The cytotoxicity of CdNCs and common BSA-AuNCs were compared by MTT assay (Figure S10a). After incubation with CdNCs or AuNCs at concentrations below 3 μM for 24 h, the viability of cells was more than 85%, indicating that CdNCs had the same good biocompatibility as AuNCs and could be employed for bioimaging. The fluorescence anti-interference ability of CdNCs was also investigated in complex intracellular environment (Fig. S10b). Fifteen common intracellular substances (amino acids and metal ions) induced less than 5% change in CdNCs fluorescence, suggesting that CdNCs were stable intracellular pH sensors. Fluorescence spectra of CdNCs in buffers with different pH

were further measured with excitation at 800 nm and 730 nm (Fig. S11). The fluorescence intensity decreased correspondingly with the increase of pH value, indicating that CdNCs maintained pH-sensitive fluorescence property under two-photon excitation. Moreover, the results of Z-Scan measurement of CdNCs at different pH values were consistent, suggesting that the pH-sensitive two-photon induced fluorescence was independent of the two-photon absorption cross section of CdNCs at 730 nm (Fig. S12).

The feasibility of CdNCs as fluorescent pH sensors was verified in living cells. The CdNCs-loaded HeLa cells were firstly treated with high K^+ buffers at different pH values containing 10 μM nigericin, which could effectively regulate the consistency of intracellular and external pH. Subsequently, the single-photon fluorescence imaging was performed on a confocal scanning microscope under 405 nm excitation. As shown in Figure S13a, the CdNCs-treated HeLa cells had obvious fluorescent signal indicating that the CdNCs were successfully internalized into the cells. Moreover, the fluorescence intensity decreased significantly with the increase of pH (Figure S13b), suggesting that CdNCs were effective fluorescent pH sensors. The UV light excitation was known to be unsuitable for practical bioimaging due to its induction of endogenous fluorescence and cellular phototoxicity. Benefiting from the excellent two-photon excited fluorescence properties, the excitation wavelength of CdNCs could be easily shifted to the NIR region by two-photon fluorescence imaging. The two-photon excited fluorescence images of intracellular pH were captured under 730 nm excitation. As shown in Figure 4, CdNCs-loaded cells had bright two-photon induced fluorescence emission, and the fluorescence intensity was linearly correlated with pH value within physiological range, indicating that the CdNCs could be employed as excellent two-photon excitation fluorescent sensors for intracellular pH.

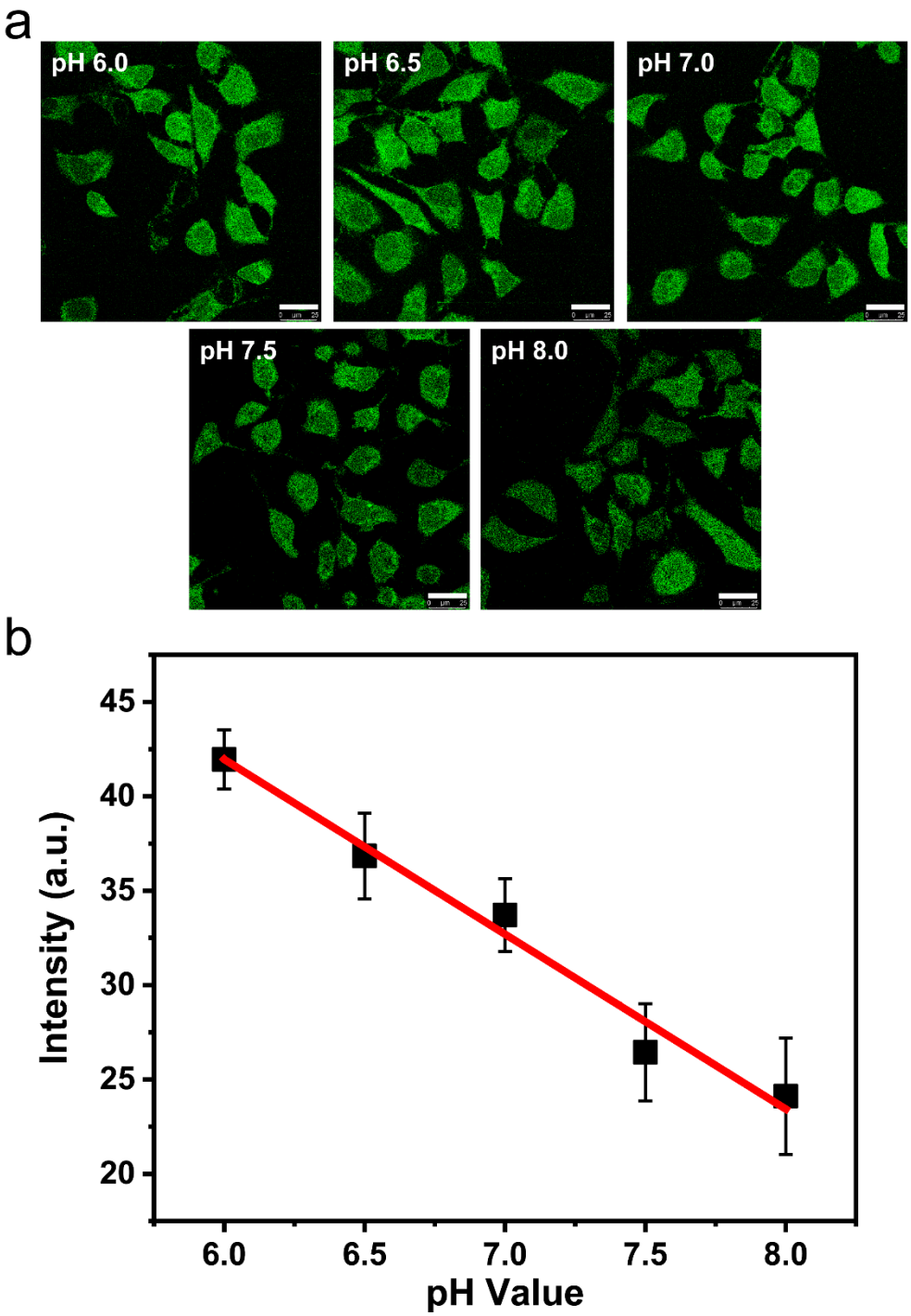

Figure 4. Intracellular pH calibration via the CdNCs. (a) Two-photon excitation fluorescence imaging of HeLa cells at different pH values (Hela cells were treated by 1.5 μM CdNCs, Ex@730 nm, Det: 500-560 nm, Scale bar: 25 μm). (b) the liner curve between fluorescence intensity and pH, Error bars: standard deviation, n = 9.

4. Conclusion

In summary, we developed a rapid one-pot route to synthesize high cadmium

content nanoclusters (CdNCs) employing bovine serum albumin (BSA) as both reducing and templating agents. The synthesized CdNCs had fluorescence quantum yield of 13.8%, and excellent two-photon absorption cross section up to 1076 GM. CdNCs also exhibited obvious pH-sensitive photoluminescence and the pH-responsive mechanism was elucidated by time-resolved fluorescence spectra and transient absorption spectra. The fluorescence of CdNCs consisted of a fast and a slow component with lifetimes of ~20 ns and ~150 ns, which were attributed to prompt fluorescence and delayed fluorescence. The delayed fluorescence was related to the Cd-S motifs structure in CdNCs. The increased pH affected the Cd-S motif structure, resulting in lower triplet state formation yield and enhanced non-radiative pathway, leading to weaker fluorescence emission and shorter lifetime of CdNCs. Furthermore, we explored the application of CdNCs in two-photon excited fluorescence intracellular pH imaging. We hope that our findings are helpful for understanding the photophysical properties of CdNCs and developing low-cost MNCs sensors based on NIR-excitation for practical biosensing.

Appendix A. Supplementary data

Experimental methods and data analysis, Supplementary Figures S1−S13 and Supplementary Tables S1-S2 (PDF)

Author Information

Corresponding Author

* Correspondence to R.A (email: rodolphe.antoine@univ-lyon1.fr) and S.Z. (email: sjzhang@phy.ecnu.edu.cn)

Acknowledgements

This work was supported by the National Natural Science Foundation of China (12174114 and 21827814), Shanghai Science and Technology Innovation Program (22520712500), “the Research Funds of Happiness Flower ECNU (2021ST2110)”, and “the Fundamental Research Funds for the Central Universities”.

References

Albota, M.A., Xu, C., Webb, W.W., 1998. Two-Photon Fluorescence Excitation Cross Sections of Biomolecular Probes from 690 to 960 nm. Appl Opt 37(31), 7352-7356.

Algar, W.R., Massey, M., Rees, K., Higgins, R., Krause, K.D., Darwish, G.H., Peveler, W.J., Xiao, Z., Tsai, H.-Y., Gupta, R., Lix, K., Tran, M.V., Kim, H., 2021. Photoluminescent Nanoparticles for Chemical and Biological Analysis and Imaging. Chem. Rev. 121(15), 9243-9358.

Ashton, T.D., Jolliffe, K.A., Pfeffer, F.M., 2015. Luminescent probes for the bioimaging of small anionic species in vitro and in vivo. Chem. Soc. Rev. 44(14), 4547-4595.

Bonacic-Koutecky, V., Antoine, R., 2019. Enhanced two-photon absorption of ligated silver and gold nanoclusters: theoretical and experimental assessments. Nanoscale 11(26), 12436-12448.

Cao, X.L., Li, H.W., Yue, Y., Wu, Y.Q., 2013. pH-Induced conformational changes of BSA in fluorescent AuNCs@BSA and its effects on NCs emission. Vib. Spectrosc. 65, 186-192.

Dong, L.Y., Li, M.L., Zhang, S., Li, J., Shen, G., Tu, Y., Zhu, J., Tao, J., 2015. Cytotoxicity of BSA-Stabilized Gold Nanoclusters: In Vitro and In Vivo Study. Small 11(21), 2571-2581.

Ghosh, S., Anand, U., Mukherjee, S., 2014. Luminescent Silver Nanoclusters Acting as a Label-Free Photoswitch in Metal Ion Sensing. Anal. Chem. 86(6), 3188-3194.

Goswami, N., Baksi, A., Giri, A., Xavier, P.L., Basu, G., Pradeep, T., Pal, S.K., 2014. Luminescent iron clusters in solution. Nanoscale 6(3), 1848-1854.

Greenfield, N.J., 2006. Using circular dichroism spectra to estimate protein secondary structure. Nature Protocols 1(6), 2876-2890.

Guo, Y., Amunyela, H.T.N.N., Cheng, Y., Xie, Y., Yu, H., Yao, W., Li, H.-W., Qian, H., 2021. Natural protein-templated fluorescent gold nanoclusters: Syntheses and applications. Food Chemistry 335.

Han, J.Y., Burgess, K., 2010. Fluorescent Indicators for Intracellular pH. Chem. Rev. 110(5), 2709-2728.

Harshita, Park, T.-J., Kailasa, S.K., 2023. Microwave assisted synthesis of blue fluorescent molybdenum nanoclusters with maltose-cysteine Schiff base for detection of myoglobin and gamma-aminobutyric acid in biofluids. Luminescence : the journal of biological and chemical luminescence.

Hu, L.Z., Han, S., Parveen, S., Yuan, Y.L., Zhang, L., Xu, G.B., 2012. Highly sensitive fluorescent detection of trypsin based on BSA-stabilized gold nanoclusters. Biosens. Bioelectron. 32(1), 297-299.

Hu, X., Mao, X.X., Zhang, X.D., Huang, Y.M., 2017. One-step synthesis of orange fluorescent copper nanoclusters for sensitive and selective sensing of Al3+ ions in food samples. Sens. Actuator B-Chem. 247, 312-318.

Iman Zare, D.M.C., Anna Cifuentes-Rius, Nasrin Moradi, Yunlei Xianyu, Subhadip Ghosh, Laura Trapiella-Alfonso, Ye Tian, Alireza Shourangiz-Haghighi, Saptarshi Mukherjee, Kelong Fan, Michael R. Hamblin, 2021. Protein-protected metal nanoclusters as diagnostic and therapeutic platforms for biomedical applications. Mater Today.

Ivleva, E.A., Obraztsova, E.A., Pavlova, E.R., Morozova, O.V., Ivanov, D.G., Kononikhin, A.S., Klinov, D.V., 2020. Albumin-stabilized fluorescent metal nanoclusters: fabrication,

physico-chemical properties and cytotoxicity. Mater. Des. 192, 8.
Li, D., Zhao, Y.Q., Chen, Z.H., Mei, X.F., Qiu, X.Z., 2017. Enhancement of fluorescence brightness and stability of copper nanoclusters using Zn2+ for ratio-metric sensing of S2. Materials Science & Engineering C-Materials for Biological Applications 78, 653-657.
Maity, A., Kumar, A., 2022. Higher-order assembly of BSA gold nanoclusters using supramolecular host-guest chemistry: a 40% absolute fluorescence quantum yield. Nanoscale Adv. 4(14), 2988-2991.
Makarov, N.S., Drobizhev, M., Rebane, A., 2008. Two-photon absorption standards in the 550-1600 nm excitation wavelength range. Opt. Express 16(6), 4029-4047.
Miao, H., Feng, Y.J., Zhong, D., Yang, X.M., 2016. Enhanced-fluorescence of europium-copper nanoclusters for cell imaging. J. Mater. Sci. 51(15), 7229-7235.
Mohanty, J.S., Xavier, P.L., Chaudhari, K., Bootharaju, M.S., Goswami, N., Pal, S.K., Pradeep, T., 2012. Luminescent, bimetallic AuAg alloy quantum clusters in protein templates. Nanoscale 4(14), 4255-4262.
Niu, Y.X., Ding, T., Liu, J.M., Zhang, G.L., Tong, L.L., Cheng, X.F., Yang, Y.M., Chen, Z.Z., Tang, B., 2021. Fluorescence switch of gold nanoclusters stabilized with bovine serum albumin for efficient and sensitive detection of cysteine and copper ion in mice with Alzheimer 's disease. Talanta 223, 6.
Olesiak-Banska, J., Waszkielewicz, M., Obstarczyk, P., Samoc, M., 2019. Two-photon absorption and photoluminescence of colloidal gold nanoparticles and nanoclusters. Chem. Soc. Rev. 48(15), 4087-4117.
Qian, H.F., Sfeir, M.Y., Jin, R.C., 2010. Ultrafast Relaxation Dynamics of Au-25(SR)(18) (q) Nanoclusters: Effects of Charge State. J. Phys. Chem. C 114(47), 19935-19940.
Qian, S.Y., Wang, Z.P., Zuo, Z.X., Wang, X.M., Wang, Q., Yuan, X., 2022. Engineering luminescent metal nanoclusters for sensing applications. Coordination Chemistry Reviews 451, 25.
Qiao, Z., Zhang, J., Hai, X., Yan, Y., Song, W., Bi, S., 2021. Recent advances in templated synthesis of metal nanoclusters and their applications in biosensing, bioimaging and theranostics. Biosens. Bioelectron. 176.
Ramakrishna, G., Varnavski, O., Kim, J., Lee, D., Goodson, T., 2008. Quantum-sized gold clusters as efficient two-photon absorbers. Journal of the American Chemical Society 130(15), 5032-+.
Russier-Antoine, I., Bertorelle, F., Vojkovic, M., Rayane, D., Salmon, E., Jonin, C., Dugourd, P., Antoine, R., Brevet, P.F., 2014. Non-linear optical properties of gold quantum clusters. The smaller the better. Nanoscale 6(22), 13572-13578.
Sarparast, M., Noori, A., Ilkhani, H., Bathaie, S.Z., El-Kady, M.F., Wang, L.J., Pham, H., Marsh, K.L., Kaner, R.B., Mousavi, M.F., 2016. Cadmium nanoclusters in a protein matrix: Synthesis, characterization, and application in targeted drug delivery and cellular imaging. Nano Research 9(11), 3229-3246.
Shi, H., Ou, M.Y., Cao, J.P., Chen, G.F., 2015. Synthesis of ovalbumin-stabilized highly fluorescent gold nanoclusters and their application as an Hg2+ sensor. Rsc Advances 5(105), 86740-86745.
Sobhan Chatterjeea, X.-Y., FengLiang, Ying-WeiYang, 2022. Surface-functionalized gold and silver nanoparticles for colorimetric and fluorescent sensing of metal ions and biomolecules,

Coordination Chemistry Reviews.
Wang, B.Q., Gui, R.J., Jin, H., He, W.J., Wang, Z.H., 2018. Red-emitting BSA-stabilized copper nanoclusters acted as a sensitive probe for fluorescence sensing and visual imaging detection of rutin. Talanta 178, 1006-1010.
Wang, T., Xiao, D., 2021. Rapid synthesis of fluorescent bovine serum albumin-gold nanoclusters complex for glutathione determination. Microchim. Acta 188(6), 193.
Wang, X.Y., Del Guerzo, A., Schmehl, R.H., 2004. Photophysical behavior of transition metal complexes having interacting ligand localized and metal-to-ligand charge transfer states. Journal of Photochemistry and Photobiology C-Photochemistry Reviews 5(1), 55-77.
Wang, Y., Nie, L., Hua, Y., Gong, L., Qiu, X., Guo, H., 2023. A simple paper-based nickel nanocluster-europium mixed ratio fluorescent probe for rapid visual sensing of tetracyclines. Spectrochimica acta. Part A, Molecular and biomolecular spectroscopy 292, 122431.
Wei, Y.F., Luan, W.L., Gao, F., Hou, X.Y., 2019. Supramolecules-Guided Synthesis of Brightly Near-Infrared Au-22 Nanoclusters with Aggregation-Induced Emission for Bioimaging. Particle & Particle Systems Characterization 36(12), 8.
Wei, Z.R., Pan, Y.T., Hou, G.J., Ran, X., Chi, Z., He, Y.L., Kuang, Y.M., Wang, X.J., Liu, R.M., Guo, L.J., 2022. Excellent Multiphoton Excitation Fluorescence with Large Multiphoton Absorption Cross Sections of Arginine-Modified Gold Nanoclusters for Bioimaging. ACS Appl. Mater. Interfaces, 12.
Wen, X.M., Yu, P., Toh, Y.R., Hsu, A.C., Lee, Y.C., Tang, J., 2012. Fluorescence Dynamics in BSA-Protected Au-25 Nanoclusters. J. Phys. Chem. C 116(35), 19032-19038.
Wu, B.Y., Wang, C.W., Chen, P.C., Chang, H.T., 2017. Glutathione assisted preparation of gold nanoclusters using minimum amount of protein. Sens. Actuator B-Chem. 238, 1258-1265.
Wu, D., Sedgwick, A.C., Gunnlaugsson, T., Akkaya, E.U., Yoon, J., James, T.D., 2017. Fluorescent chemosensors: the past, present and future. Chem. Soc. Rev. 46(23), 7105-7123.
Xavier, P.L., Chaudhari, K., Baksi, A., Pradeep, T., 2012. Protein-protected luminescent noble metal quantum clusters: an emerging trend in atomic cluster nanoscience. Nano reviews 3.
Xie, J.P., Lee, J.Y., Wang, D.I.C., Ting, Y.P., 2007. Silver nanoplates: From biological to biomimetic synthesis. ACS Nano 1(5), 429-439.
Xie, J.P., Zheng, Y.G., Ying, J.Y., 2009. Protein-Directed Synthesis of Highly Fluorescent Gold Nanoclusters. Journal of the American Chemical Society 131(3), 888-+.
Xu, C., Webb, W.W., 1996. Measurement of two-photon excitation cross sections of molecular fluorophores with data from 690 to 1050 nm. J. Opt. Soc. Am. B-Opt. Phys. 13(3), 481-491.
Zhao, Y., Hu, Q., Cheng, F., Su, N., Wang, A., Zou, Y., Hu, H., Chen, X., Zhou, H.-M., Huang, X., Yang, K., Zhu, Q., Wang, X., Yi, J., Zhu, L., Qian, X., Chen, L., Tang, Y., Loscalzo, J., Yang, Y., 2015. SoNar, a Highly Responsive NAD(+)/NADH Sensor, Allows High-Throughput Metabolic Screening of Anti-tumor Agents. Cell Metabolism 21(5), 777-789.
Zheng, J., Zhang, C.W., Dickson, R.M., 2004. Highly fluorescent, water-soluble, size-tunable gold quantum dots. Phys. Rev. Lett. 93(7), 4.
Zhou, M., Jin, R., 2021. Optical Properties and Excited-State Dynamics of Atomically Precise Gold Nanoclusters, in: Johnson, M.A., Martinez, T.J. (Eds.), Annual Review of Physical

Chemistry, Vol 72. pp. 121-142.
Zhou, Q., Lin, Y.X., Xu, M.D., Gao, Z.Q., Yang, H.H., Tang, D.P., 2016. Facile Synthesis of Enhanced Fluorescent Gold-Silver Bimetallic Nanocluster and Its Application for Highly Sensitive Detection of Inorganic Pyrophosphatase Activity. Anal. Chem. 88(17), 8886-8892.